Nuclear Materials and Energy 45 (2025) 102018

Contents lists available at ScienceDirect

Nuclear Materials and Energy

journal homepage: www.elsevier.com/locate/nme

Ultrathin boron layer (a few nm to 100 nm) diagnostics on tungsten substrates via spatiotemporally resolved picosecond LIBS in a vacuum☆

Huace Wu [a,b], Rongxing Yi [b], Sebastijan Brezinsek [b,*], Anne Houben [b], Marcin Rasinski [b], Rui Ding [c], Matej Mayer [d], Gennady Sergienko [b], Timo Dittmar [b], Hongbin Ding [e,*]

[a] Institute of Energy, Hefei Comprehensive National Science Center (Anhui Energy Laboratory), 230031 Hefei, PR China
[b] Institute of Fusion Energy and Nuclear Waste Management – Plasma Physics, Forschungszentrum Jülich 52425 Jülich, Germany
[c] Institute of Plasma Physics, Chinese Academy of Sciences, 230031 Hefei, PR China
[d] Max-Planck-Institute für Plasmaphysik, 85748 Garching, Germany
[e] School of Physics, Dalian University of Technology, 116024 Dalian, PR China

ARTICLE INFO

Keywords:
Boronization
Ps-LIBS
Boron-films on W-substrates
Quantitative calibration curve
Limit-of-detection

ABSTRACT

The impact of the thickness and uniformity of boron (B) layer deposited by the boronization process, as well as the understanding of the layer's lifetime and oxygen gettering effectivity, remains uncertain and real time diagnosis is required in future. Building upon our previous work, the picosecond laser-induced breakdown spectroscopy (ps-LIBS) technology with spatial resolution capability was further employed to detect B elements in B films deposited on tungsten (W)-substrates samples. By adjusting experimental parameters such as laser energy and spot size, and studying the spatiotemporal evolution of W and B elements, the optimal experimental parameters were determined. Under a laser spot diameter of 488 μm, a laser fluence of 9.6 J/cm^2, a delay time of 30 ns, and a gate width of 600 ns were used to improve the limit of detection (LOD) of B by ps-LIBS. A set of samples with different B layer thicknesses on W-substrates from 5.6 to 151.5 nm was obtained through exposure of samples by magnetron sputtering in a laboratory arrangement and exposure of samples on a manipulator during two boronizations in the stellarator W7-X. The thickness of the B layers was measured by Focused Ion Beam combined with Scanning Electron Microscopy (FIB-SEM) and Nuclear Reaction Analysis (NRA). After extracting the net B signal from the LIBS spectra, a quantitative calibration curve and LOD of the B II-703.2 nm for the B layers on W-substrates were established for the first time. These results confirm that ps-LIBS technology holds promise for *in situ* diagnostics of ultrathin B layers, ranging from a few nm to 100 nm, on W-substrates in fusion devices after boronization.

1. Introduction

Boronization has been applied and developed in tokamak devices since the 1980s [1–3], and later in stellarator/helical devices as well [4,5]. The effects of boronization wall conditioning are primarily reflected in three aspects: gettering the oxygen (O) and reduce the release of impurities, inhibiting the release of high-Z metals from metallic vessel walls wall; and lowering the particle recycling of hydrogen and its isotopes [6–8]. According to the revised plan in 2024, the first wall material in ITER is planned be changed from beryllium (Be) to tungsten (W) [9]. This material change brings new challenges: firstly, tungsten as the first wall will be exposed at the main chamber wall, and eroded tungsten from the main chamber has a lower screening efficiency in comparison with to tungsten originating from the divertor, thus, the pollution of the core confinement is possible. Secondly, with the removal of Be's oxygen-gettering ability, substitute measures may be needed to reduce the partial pressures of impurities such as water (H_2O) and O [10]. Given these challenges, boronization is currently considered as wall conditioning method in ITER to ensure a smooth first start-up of plasma operation and subsequently to achieve the scientific goals of ITER including Q = 10 operation under steady-state conditions.

Currently, before high-parameter plasma operations, the vaporized carborane ($C_2B_{10}H_{12}$) [11], decaborane ($B_{10}D_{14}$) [12], or diborane (B_2H_6) [13] gas is typically used as the working gas in a glow discharge

☆ This article is part of a special issue entitled: 'PFMC-20' published in Nuclear Materials and Energy.
* Corresponding authors.
E-mail addresses: s.brezinsek@fz-juelich.de (S. Brezinsek), hding@dlut.edu.cn (H. Ding).

https://doi.org/10.1016/j.nme.2025.102018
Received 22 July 2025; Received in revised form 8 September 2025; Accepted 28 October 2025
Available online 31 October 2025

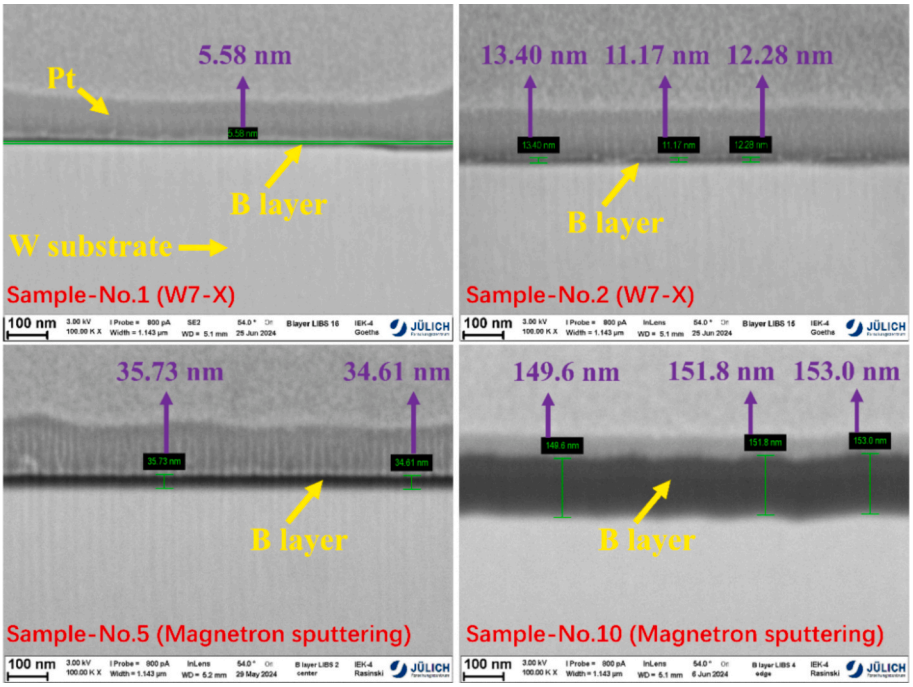

Fig. 1. The cross-section of several typical samples obtained by FIB-SEM.

(GD) or ion cyclotron range of frequency (ICRF) discharge. The B compounds are dissociated to coat the plasma-facing materials (PFMs) with B layer. Nevertheless, these B layer gradually saturate or erode with prolonged exposure to high-parameter plasma. Complementary, the real-time wall conditioning technologies, such as the impurity powder dropper (IPD), have been developed to achieve high-performance discharges, particularly for long-pulse plasma operations, but they can be seen as final mitigation technique [14,15].

However, recent studies by Masuzaki et al [16] indicate that the distribution of boron layers is non-uniform in both of these boronization methods. The impact of the deposited B layer thickness, and its homogeneity after the boronization process is uncertain as well as knowledge about the layer lifetime and improved conditions under non homogenous deposition, which requires real-time diagnosis. Laser-induced breakdown spectroscopy (LIBS) is considered a promising technique that can be used to *in situ* and real-time investigate the elemental composition, content, and thickness of deposited layers on the surfaces of PFMs [17]. LIBS has been successfully applied for *in situ* detection of key elements (H/D, Li, B, O, C, Si, W and so on) on several fusion devices [18–21]. While nanosecond (ns)-LIBS is commonly used, studies on W-based plasma-facing materials show that picosecond (ps)-LIBS offers clear advantages [22–24]. Its much lower ablation rate (~3–4 × lower for W) reduces heat-affected zones, melting and fractionation, preserving stoichiometry and improving depth resolution for fuel retention analysis. Moreover, the shorter pulses minimize plasma shielding and lower electron density, yielding narrower spectral lines and better spectral resolution. Owing to its excellent depth resolution and minimal thermal effects, ps-LIBS is also particularly suitable for measuring boron layers on wall surfaces at different locations after boronization [25]. Ps-LIBS has been successfully used in the laboratory to measure the B-deposition layers on the divertor tiles of the Wendelstein 7-X (W7-X) device after the OP 1.2b phase [26]. The results indicate that the distribution of B along the radial direction of the divertor after hydrogen plasma operation and material migration is not uniform and complete erosion and thick deposits can occur. At the same time, in our previous work [27], the depth distribution of B-films on W-substrates with the thicknesses of 130 nm and 260 nm were measured by ps-LIBS under the different laser spot sizes (diameter: 142–1518 μm). The interface between B-films and W-substrates, as well as the thickness of the B-films, were determined and the results from ps-LIBS measurements are in good agreement with those obtained through the Focused Ion Beam combined with Scanning Electron Microscopy (FIB-SEM) and Energy Dispersive X-ray Spectroscopy (EDS). However, if the B layer thickness is less than 100 nm, or even below the depth ablation rate of the ps-LIBS, the quantitative calibration curve and the limit of detection (LOD) for the B layer thickness need to be further established.

W7-X is an advanced stellarator with superconducting coils. Its second operational phase, OP 1.2, was subdivided into two sub-phases. Compared to OP 1.2a, which did not undergo boronization wall conditioning, W7-X performed three boronization wall conditioning during OP 1.2b [28]. The boronization was carried out in a He-GDC with 90 % He and 10 % B_2H_6. The results showed a significant decrease in the O and C concentrations in the plasma, with Z_{eff} dropping from 4.5 to 1.2. The line-integrated electron density increased from 4×10^{19} m^{-2} to above 1×10^{20} m^{-2}, and the diamagnetic energy increased from 330 kJ to 510 kJ [29]. The boronization proved to be a key factor in achieving good plasma performance. Subsequently, boronization was continued in OP 2.1. In this work, several B layer samples with different thicknesses on W-substrates were obtained from the magnetron sputtering and the 3rd and 4th boronization during OP 2.1. The thickness of the B layers on different samples was determined using FIB-SEM and Nuclear Reaction Analysis (NRA). The signals for measuring the B layers on the W substrates by ps-LIBS were then optimized. Finally, a quantitative calibration curve and LOD for the B layers on the W substrates were established.

2. Experimental setup

2.1. Sample preparation and characterization

The experiment involves four types of materials: pure W target (10 mm × 10 mm × 5 mm, double-forged W with 99.99 % purity, produced by Plansee SE according to the ITER specifications), pure B target (99.95 % purity, Mateck), the B-layer samples with different thicknesses on W-substrates obtained by magnetron sputtering, and the B-layer samples with different thicknesses on W-substrates after boronization in W7-X. Pure W and B target samples were used to determine the LIBS spectra

Table 1
The thicknesses of B-layer samples measured by FIB-SEM. Samples No.1 and No.2 also measured by the NRA.

Sample (No.)	1 (W7-X)	2 (W7-X)	3 (MS)	4 (MS)	5 (MS)
Thickness (nm)	5.6 ± 1.19 5–7 (NRA)	12.3 ± 1.12 10–15 (NRA)	14.5 ± 0.65	20.1 ± 1.29	35.2 ± 0.79
Sample (No.)	6 (MS)	7 (MS)	8 (MS)	9 (MS)	10 (MS)
Thickness (nm)	58.6 ± 0.78	84.1 ± 1.29	116.8 ± 1.27	128.4 ± 2.09	151.5 ± 1.72

of W and B elements in the 696–708 nm range as reference, as well as the spatiotemporal evolution characteristics of the plasma. This information is beneficial for distinguishing and detecting the B and W spectral lines.

Consistent with the previous work [27], a set of polished W targets was used as substrate samples for magnetron sputtering deposition. The deposition process was carried out using a pure B target under Ar plasma conditions (RF, 140 W). The thicknesses of the deposited B layers on the W-substrates were determined by varying the sputtering durations. To ensure uniform deposition of the B films, the sample holder was rotated. After deposition, the samples were removed from the vacuum chamber and stored in dry air (humidity < 40 %) at room temperature for three weeks before being transported to the LIBS and FIB-SEM laboratory for analysis. Fig. 1 presents the transverse cross-sectional images of several typical samples measured by FIB-SEM. The platinum (Pt) coating is a common and important step in FIB-SEM technology. It improves imaging quality, enhances sample stability, and protects the sample surface by reducing the damage caused by the focused ion beam. Due to the different contrast colors of Pt, B, and W-substrates under the scanning electron microscope, the boundaries between the three materials can be clearly distinguished. The samples with B layers thicknesses of approximately 14.5 nm, 20.1 nm, 35.2 nm, 58.6 nm, 84.1 nm, 116.8 nm, 128.4 nm, and 151.5 nm were obtained and the results presented in Table 1. The sample with a B layer thickness of 128.40 nm (Sample No. 9) was used to study the relationship between spectral intensity, laser spot size, and laser fluence, as shown in Fig. 5. Samples with other B layers thicknesses were used to establish the quantitative calibration curves for

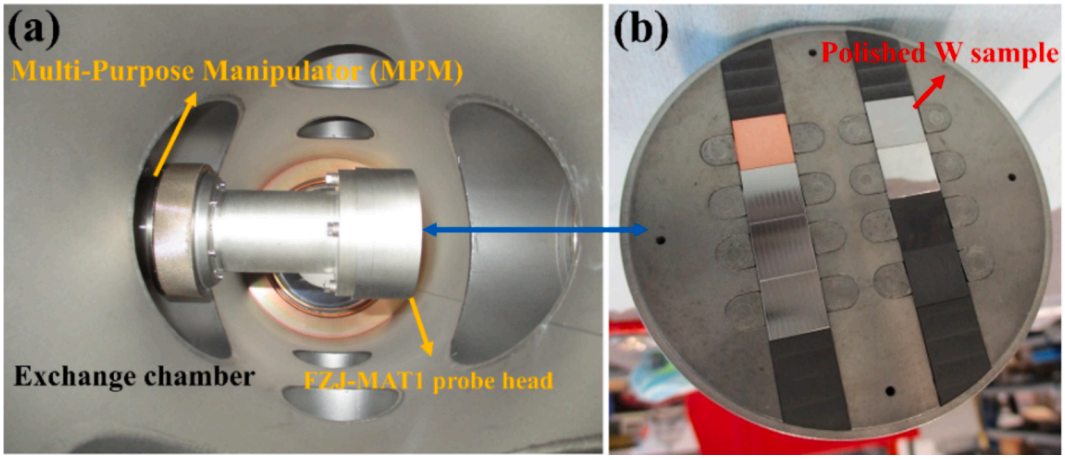

Fig. 2. (a) The photo of FZJ-MAT1 probe head mounted on MPM in the exchange chamber of W7-X. (b) The photo of FZJ-MAT1 probe head with samples installed.

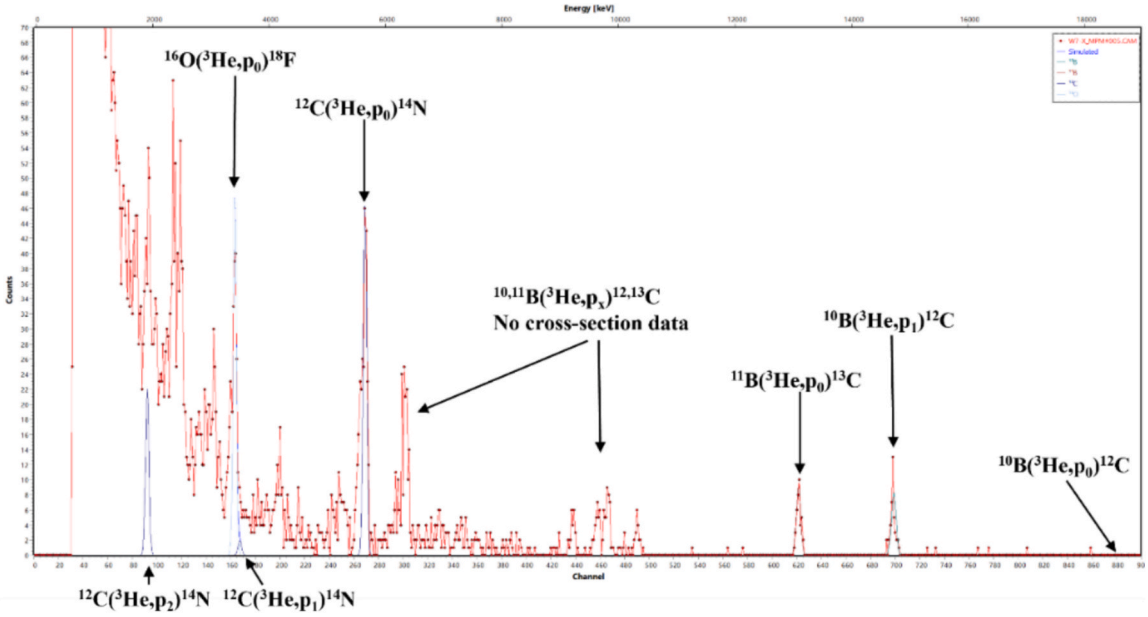

Fig. 3. The sample-No.2 spectrum of a spot measured by NRA. Peaks $^{10,11}B(^3He,p_x)^{12,13}C$, $^{12}C(^3He,p_{0,1,2})^{14}N$ and $^{16}O(^3He,p_0)^{18}F$ were labeled by comparing the original and simulated spectrum.

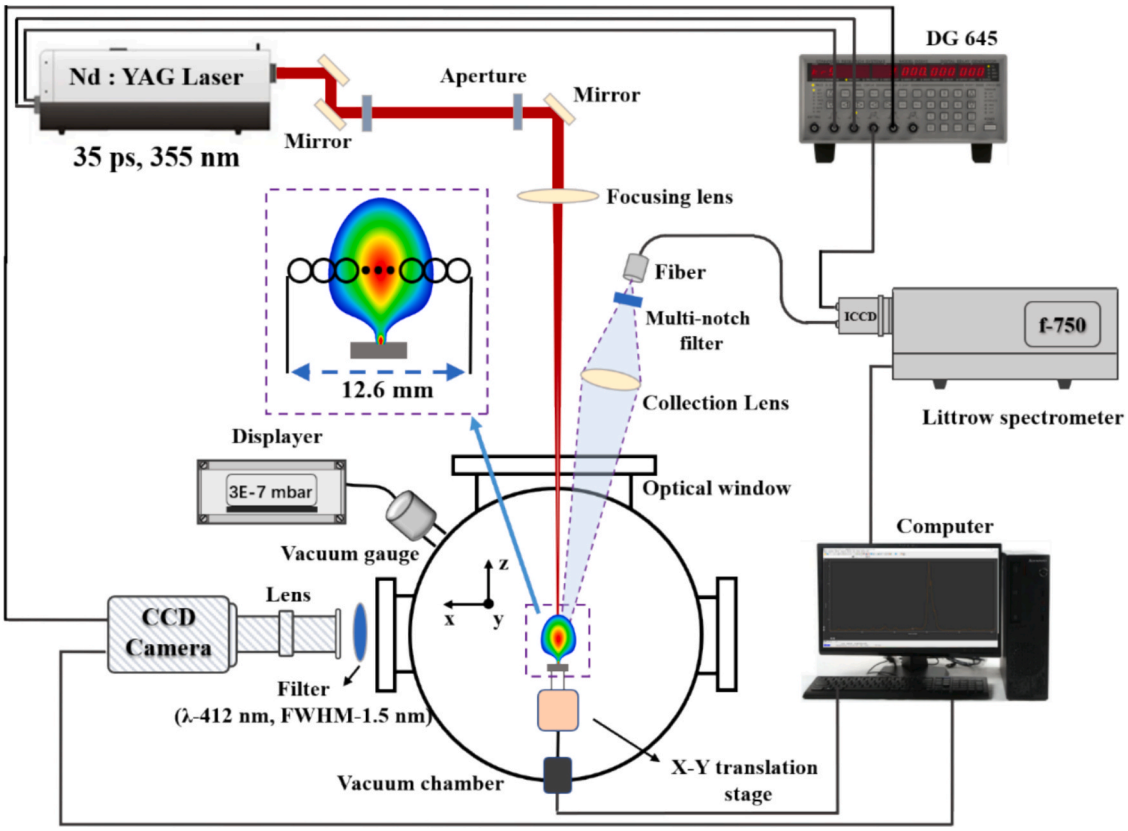

Fig. 4. Experimental set up of ps-LIBS.

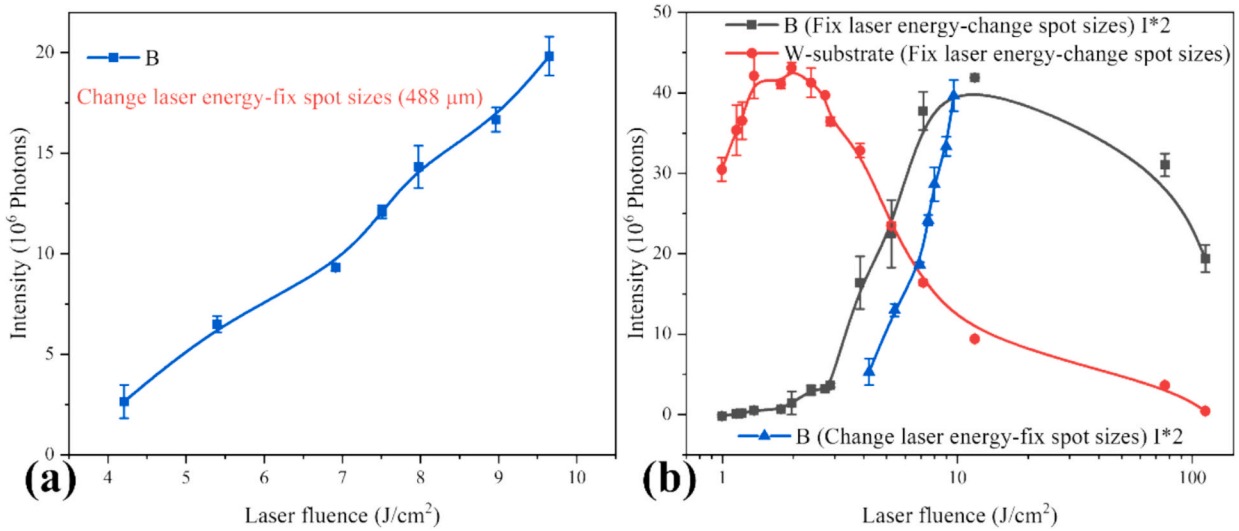

Fig. 5. (a) The emission intensity of B II-703.2 nm varies with the laser fluence. The diameter of the laser spot is fixed at 488 μm. (b) Comparison of spectral line intensity in two different cases. The black and red lines indicate that when the laser energy is fixed at 18 mJ, the emission intensity of B II-703.2 nm and W I-699.4 nm vary with the sizes of the laser spot, respectively [27]. The blue line shows that when the diameter of the laser spot is fixed at 488 μm, the emission intensity of B II-703.2 nm varies with the laser energy. (For interpretation of the references to colour in this figure legend, the reader is referred to the web version of this article.)

Table 2
Laser energy and corresponding laser fluence. The diameter of the laser spot is 488 μm.

Laser energy (mJ)	7.9	10.1	12.9	14.0	14.9	16.8	18.0
Laser fluence (J/cm^2)	4.2	5.4	6.9	7.5	8.0	9.0	9.6

B layer thickness and content.

Five boronization processes were conducted during the OP 2.1 campaign of W7-X. Eight samples (12 mm × 10 mm × 5 mm, consisting of W, C, Al, Cu, and Steel) were exposed using the multipurpose manipulator (MPM) during two boronizations in OP 2.1 (3rd boronization on 4.2.2023 and 4th boronization on 25.2.2023). A photo of the manipulator probe head with the installed samples is shown in Fig. 2. The 3rd boronization lasted 146 min, at a pressure range of 9–11 × 10^{-3}

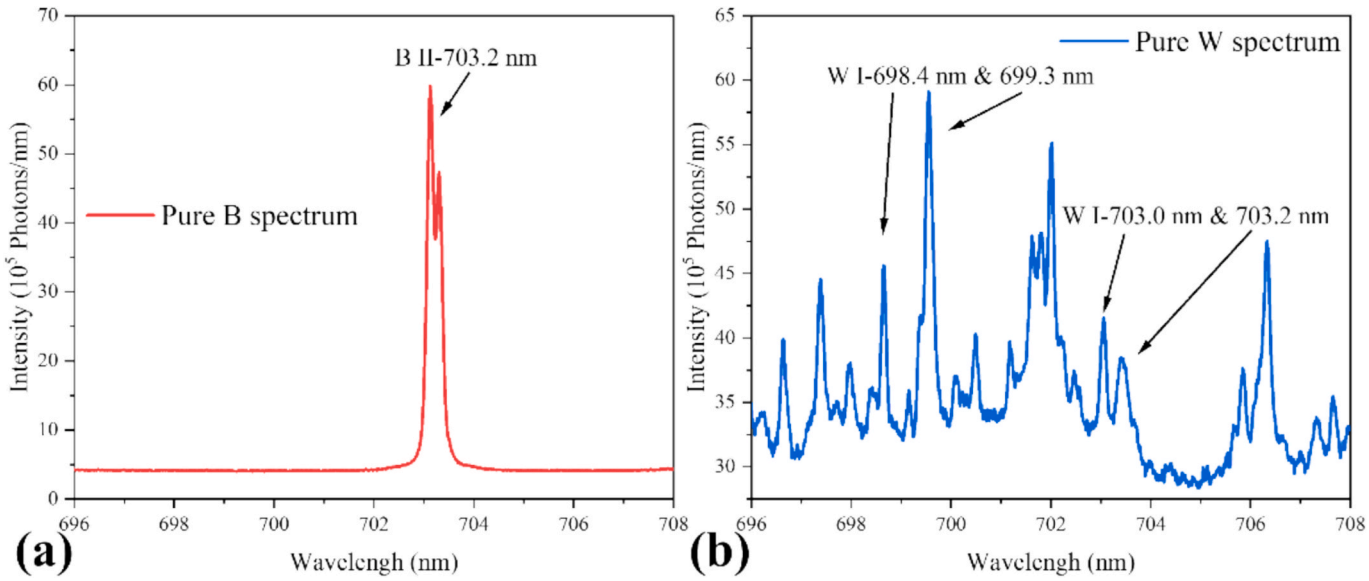

Fig. 6. LIBS spectra of (a) pure B and (b) pure W. The diameter of laser spot sizes is fixed at 488 μm (9.6 J/cm^2).

mbar, with an injected gas amount of 35.4 bar*l (electrode current:1–1.7 A). The 4th boronization lasted 190 min, at a pressure of 8×10^{-3} mbar, with an injected gas amount of 38.1 bar*l (electrode current:0.8 A). In this work, only the samples covered with B layers on W-substrates were analyzed by LIBS, and other materials were not discussed in detail. Both samples were extracted immediately after boronization and were not subjected to any subsequent plasma-discharge irradiation. The samples covered with B layers on W-substrates were stored at room temperature for about one year before being transported to the LIBS laboratory.

The polished W samples exposed during each boronization were also analyzed using NRA with 3 MeV ^{3}He ions, and the thickness measurement results also presented in Table 1. Fig. 3 presents the sample spectra measured by NRA. The peaks corresponding to ^{10,11}B(^{3}He,p$_x$)^{12,13}C, ^{12}C(^{3}He,p$_{0,1,2}$)^{14}N and ^{16}O(^{3}He,p$_0$)^{18}F were identified by comparing the experimental and simulated spectra. The detailed measurement parameters are thoroughly described in the work of Mayer et al [30]. The results indicate that, during the 3rd boronization, 10–15 $\times$ 10^{16} B-atoms/cm^2 (10–15 nm) have been deposited on the sample No. 2, while during 4th boronization, only 5–7 $\times$ 10^{16} B atoms/cm^2(5–7 nm) have been deposited on the sample No. 1.

2.2. Ps-LIBS system

Fig. 4 illustrates the experimental setup of the ps-LIBS system. The basic configuration is similar to previous work [27], with the focus placed on the sensitivity improvements made to the system. The Nd:YAG laser, with a pulse width of 35 ps and a wavelength of 355 nm (third harmonic), was focused onto the sample surface inside the vacuum chamber using a focusing lens with a diameter of 50 mm and a focal length of 500 mm. The pressure inside the vacuum chamber was maintained at 3×10^{-7} mbar, as measured by the gauge. The light from the laser-induced plasma passes through an optical window, is collected by a lens with a diameter of 75 mm and a focal length of 200 mm, and then coupled into a fiber. The plasma image was reduced by a demagnification factor of 2 by the collecting lens. Unlike the single-core fiber used in previous work [27], a linear array of fiber bundles was employed for the detection of W and B elements. This fiber bundle consists of 20 linear array fibers each with a core diameter of 350 μm, resulting in a total collection area length of approximately 14 mm and a spatial resolution of 0.7 mm. The other end of the fiber was coupled to a custom-made spectrometer with a Littrow configuration (F-number: 4.3). Thus, the signal collection system, equipped with an ICCD camera (iStar DH334T-18F, Andor) featuring gating capability and a linear array of fiber bundles, provides spatial resolution and enhances detection sensitivity [31]. A CCD camera (PIKE-F100) equipped with a narrow-band interference filter (central λ–412 nm FWHM–1.5 nm) was used to synchronously capture images of the laser-induced plasma plume. A digital delay generator (DG645, Stanford R.S.) was employed to coordinate the timing sequence of the laser, spectrometer, and CCD camera.

3. Results and discussion

3.1. Optimization of laser spot sizes and laser fluence

Before measuring the B layer samples, the optimal LIBS experimental parameters, such as laser spot size and laser fluence, need to be determined first. There are typically two common methods to change the laser fluence. The first method involves fixing the spot size and adjusting the laser energy to modify the laser fluence. The second method involves fixing the laser energy and adjusting the laser spot sizes to change the laser fluence. Understanding the variation in the signal intensity under these two conditions is of significant value for improving the LOD of B. In previous work [27], the variation in the intensity of B and W spectral lines with spot size changes under fixed laser energy was systematically investigated. The change in spot size was converted into a change in laser fluence, and the intensity trends of the B and W spectral lines are shown in Fig. 5(b) by the black and red lines, respectively. The thickness of the B layer on the W-substrate is 128.4 nm (Sample No. 9), and the spectral line intensity is the cumulative value of the laser pulses (the sum of the net B signal). The use of Sample No. 9, with an identical B-layer thickness on a W substrate, enables direct verification of the earlier results and a deeper understanding of the underlying mechanisms. Due to the different spectroscopic parameters and excitation thresholds of B II-703.2 nm and W I-699.4 nm, there is a significant difference between the two curves. However, when the laser spot size changes, both the laser fluence and spot size (the ablation amount of B) vary simultaneously, thus influencing the spectral line intensity. In this work, a comparative experiment was conducted. The diameter of laser spot size was fixed at 488 μm (the ablation amount of B is approximately constant), and the relationship between the intensity of B II-703.2 nm and laser fluence was obtained by adjusting the laser energy, as shown in Fig. 5(a). The curve was obtained by using B-spline fitting. This method provides local control and guarantees smoothness, thereby enabling a more accurate representation of the overall trend of the experimental data. The laser

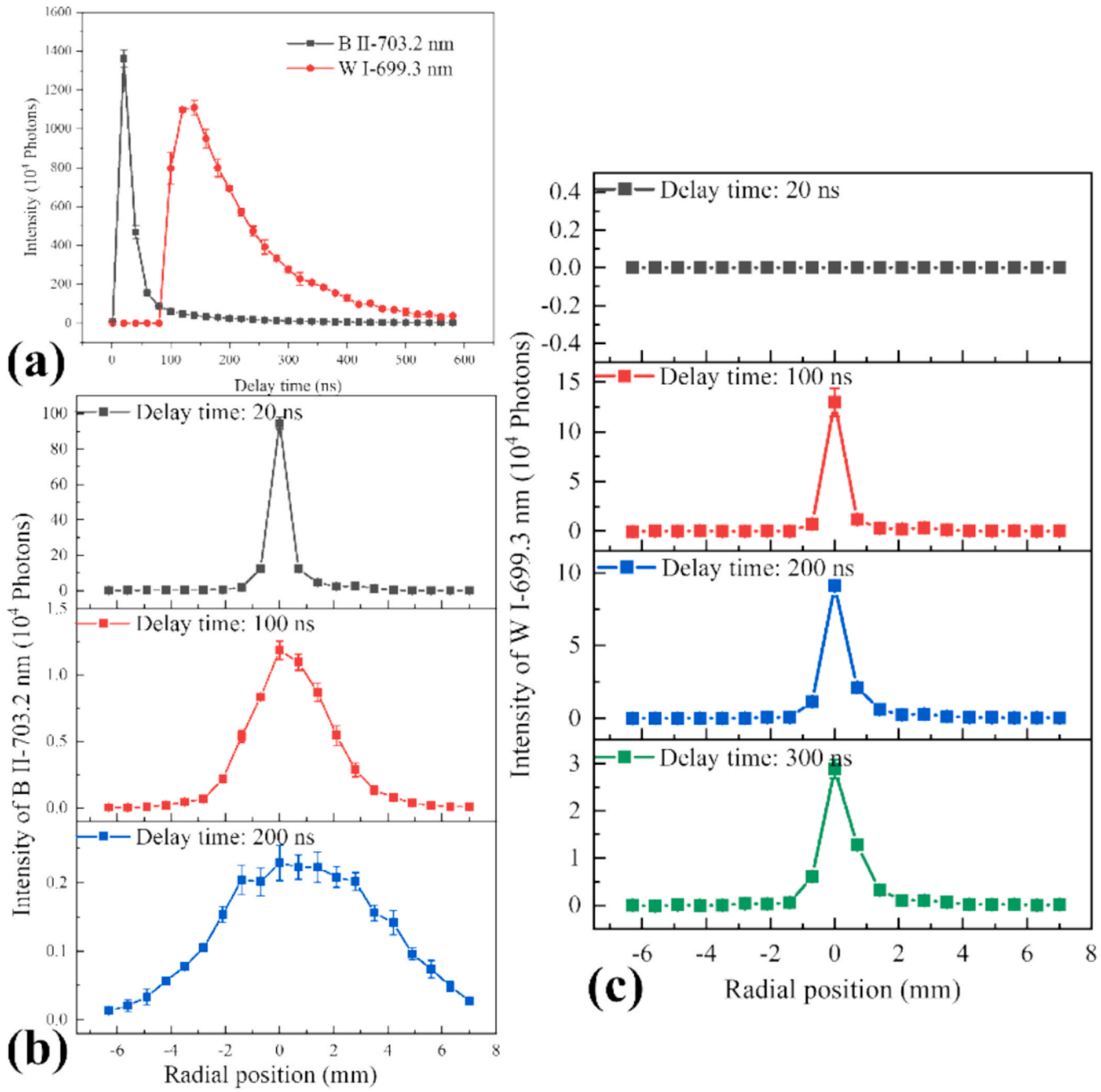

Fig. 7. (a) Temporal evolution of intensities of B II-703.2 nm and W I-699.4 nm. The delay time = 0 is synchronized with the laser pulse. The spatiotemporal distribution characteristics of (b) B II-703.2 nm and (c) W I-699.4 nm. The diameter of laser spot sizes is fixed at 488 μm (9.6 J/cm^2).

energy and corresponding laser fluence used in this work are shown in Table 2.

The intensity of B II-703.2 nm increases significantly with laser fluence. It is reasonable that when the B ablation amount is fixed, an increase in laser fluence effectively raises the plasma temperature (T_e) and the electron density (n_e), thereby enhancing the spectral line intensity [32]. This result is plotted in Fig. 5(b) as the blue line. The result shows that, for the same laser fluence (<9.6 J/cm^2), the intensity value of the black line is consistently higher than that of the blue line. Comparing the spectral intensities under the two methods, although the laser fluence is the same, the number of B atoms ablated with the changing spot size is greater than the number ablated when the spot size is fixed. This directly confirms the explanation provided in previous work regarding the trend of B intensity variation with changes in spot size [27]. Specifically, although the laser fluence decreases with the increasing spot size, the ablation amount increases as the spot size grows, which is the result of the combined effects of these two factors.

Based on the results shown in Fig. 5(b), the LIBS experimental parameters were optimized with a laser spot diameter of 488 μm and a laser fluence of 9.6 J/cm^2 to achieve the optimal LOD for B under the current experimental conditions.

3.2. *Photon number of characteristic lines and spatiotemporal evolution of B and W*

An absolute calibration method was employed to convert the intensity values of the characteristic spectral lines into the number of photons collected within a specific solid angle, as expressed in Eqn. (1)

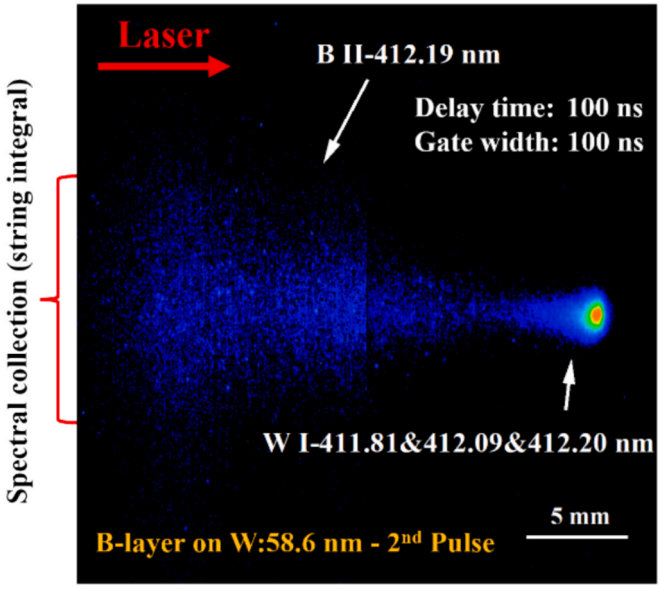

Fig. 8. The photograph of the laser-induced plasma by the CCD camera. A narrow band filters (central λ-412 nm FWHM-1.5 nm) was used to investigate the plasma emission of B II and W I characteristic lines. The diameter of laser spot sizes was fixed at 488 μm (9.6 J/cm^2).

[33].

$$I(\lambda_{ki}) = Đ¤(\lambda_{ki})L(\lambda_{ki})D(\lambda_{ki},\ g)K(\lambda_{ki}) \quad (1)$$

where λ_{ki} is the wavelength of the characteristic line, $I(\lambda_{ki})$ represents the photon number of characteristic lines, $Đ¤(\lambda_{ki})$ is the integrated plasma radiance, accounting for any relaying optics, $L(\lambda_{ki})$ denotes the counts obtained by spectrometer, $D(\lambda_{ki},\ g)$ is the detector response, such as gain, and $K(\lambda_{ki})$ is the conversion factor with units of photons per count. All of these parameters are functions of the λ_{ki}. The detailed steps of this method have been thoroughly described in previous work [34]. In this work, the solid angle for signal collection is approximately 0.0276 sr. The counts of the characteristic line radiation obtained by the spectrometer were all converted into the number of photons.

Fig. 6 presents the laser-induced plasma spectra of pure B and pure W. Due to the differences in the number of electrons in the outer shells of the atoms and their transition rules, the spectra of these two elements show significant difference. In the 696–708 nm range, only B II-703.02 nm, 703.19 nm, and 703.25 nm can be detected for the B element, while the W element exhibits a more densely packed set of W I lines. It can be observed that both B and W elements have lines near 702 nm, indicating that there will be an overlapping spectral region when measuring the B layers on W-substrates using LIBS.

In previous work [27], the temporal evolution behaviors of B and W were systematically studied, and the radiative lifetimes of the characteristic lines of B and W elements were estimated. To further understand the plasma dynamics of B and W elements, and to optimize detection parameters for better LOD, this work presents an in-depth study of the spatiotemporal evolution behavior of B and W. The gate delay was set to $20 \times n$, where n is the number of measurement steps. The gate integration time was fixed at 20 ns. The collection method was along the laser direction with a paraxial collection angle of 15°, as shown in Fig. 4. Fig. 7(a) presents the temporal evolution of the intensities of B II-703.2 nm and W I-699.3 nm. The delay time = 0 is synchronized with the laser pulse.

The spatiotemporal distribution characteristics of B II-703.2 nm and W I-699.4 nm obtained using the linear array fibers are shown in Figs. 7 (b) and (c), respectively. The radiation lifetime of the spectral characteristic line is influenced by various factors, including the upper energy level (E_k), transition probability (A_{ki}), and plasma parameters (T_e and n_e). The lifetime of B II-703.2 nm (E_k:17.85 eV) is relatively short, which can be attributed to the rapid decrease in T_e and n_e following laser ablation in a vacuum. At the same time, due to the effects of mass and sheath acceleration, the spatiotemporal distribution behaviors of B II-703.2 nm and W I-699.4 nm differ significantly [31]. At a delay time of 20 ns, the B II signal is already detected, while the W I signal has not yet appeared. At a delay time of 100 ns, the radial diameter of the spatial profile of B II exceeds 6 mm (the boundary is determined by 10 % of the maximum intensity), while the radial diameter of the spatial profile of W I is less than 2.5 mm. At a delay time of 200 ns, the radial diameter of the spatial profile of B II exceeds 12 mm, while the radial diameter of the spatial profile of W I remains smaller than 3.5 mm. Due to the spectral collection is paraxial rather than coaxial, the spatial distribution profiles of B II and W I are not perfectly symmetrical.

To further validate the spatiotemporal evolution results of the LIBS spectra, a fast plasma imaging method was used to capture the laser-induced plasma. The CCD camera, positioned perpendicular to the laser incident direction, recorded the plasma plume image of sample No. 2(B-layer:58.6 nm) under the 2nd laser pulse, as shown in Fig. 8. Both the B layer and the W substrate were ablated at the 2nd laser pulse, as evidenced by Fig. 9(b). A narrowband interference filter (central λ-412 nm FWHM-1.5 nm) was used to image the plasma emission of B II and W I characteristic lines. The recorded delay time and gate integration time were both 100 ns. At this moment, the B II emission cloud is clearly more expanded and extends farther than the W I emission cloud. Compared to atoms, univalent ions typically exhibit faster expansion to farther regions due to the acceleration from the sheath electric field in the shorter time following laser ablation. Additionally, the relative atomic masses of B and W are 10.81 and 183.84, respectively. Such a large mass difference results in a higher expansion speed for B compared to W. Therefore, at the same delay time, the spatial distribution profile of B is significantly wider than that of W. The emission behavior of the plasma plume recorded by the CCD is consistent with the spatiotemporal evolution behavior observed in the spectra.

Based on the above phenomena, this work determined the signal acquisition parameters with a delay time of 30 ns, gate integration time of 600 ns, and a collection region length of 14 mm to achieve the measurement of the B layers on the W-substrates. Furthermore, the significant spatial distribution differences between B and W will aid in distinguishing the spectral overlap region between B II-703.2 nm and W I-703.0 nm&703.2 nm, which will be discussed in Section 3.3.

3.3. The LIBS spectra under different laser pulses and the distinction between the B and W characteristic lines

Fig. 9 presents the LIBS spectra of B layer samples with different thicknesses on W-substrates as a function of the number of laser pulses. The spectrum obtained for each laser pulse is the result of spatial integration (the sum of the 20 fibers). Fig. 9(a) shows the LIBS spectra of sample No. 1 for the first three laser pulses. It can be seen that, due to the B layer being only 5.6 nm thick, the 1st laser pulse ablates the W substrate (the strongest W I peaks such as W I-698.4 nm & 699.3 nm are detected), and the region around 703.2 nm represents the overlap region between B II and W I. The LIBS spectra obtained from the 2nd and 3rd laser pulses are nearly identical, indicating that the B layer has been removed by the 1st laser pulse. However, as the B layer thickness increases, the spectral features under different laser pulses show significant changes. Fig. 9(b) presents the LIBS spectra corresponding to sample No. 6, which has a B layer thickness of 58.6 nm. Under the 1st laser pulse, only the B signal is detected, with no signal from the W-substrate. Comparing the LIBS spectra obtained from the 2nd, 3rd, and 4th laser pulses, it is evident that the B and W-substrate signals both appear under the 2nd laser pulse. After two laser pulses, the B layer on the W-substrate is completely removed. For sample No.10, with a B layer thickness of 151.5 nm, the LIBS spectra show only the B signal without

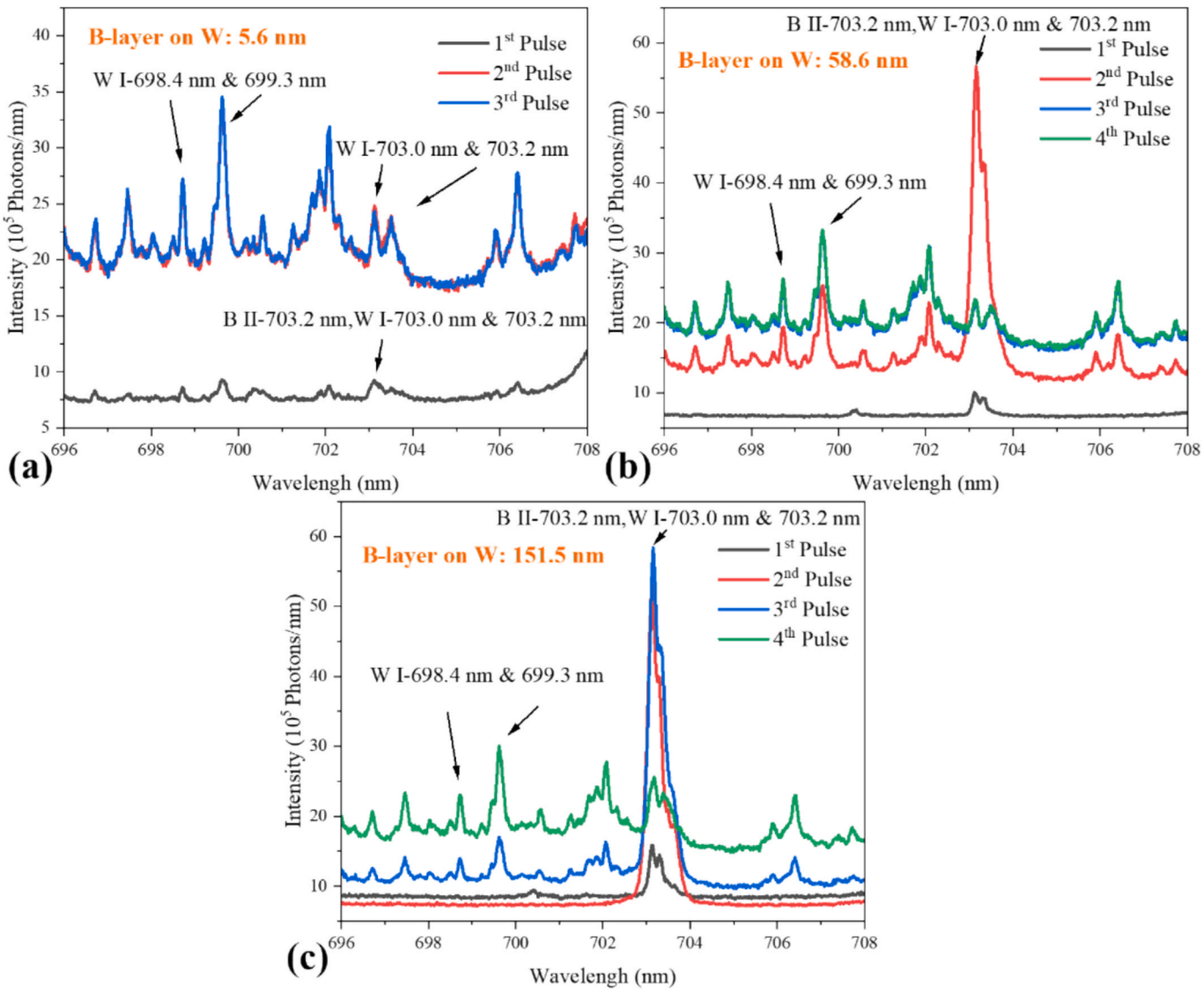

Fig. 9. The spectra of B layers about (a) 5.6 nm (sample-No.1), (b) 58.6 nm (sample-No.6) and (c) 151.5 nm (sample-No.10) on the W-substrates under different laser pulses, respectively. The diameter of laser spot sizes is fixed at 488 μm (9.6 J/cm^2).

any W-substrate signal under the first two laser pulses, as shown in Fig. 9 (c). The spectrum obtained from the 3rd laser pulse exhibits a strong B signal and a weak W-substrate signal, while the spectrum from the 4th laser pulse shows a weaker B signal and a stronger W-substrate signal. This indicates that the 3rd laser pulse ablated a larger amount of B, while the 4th laser pulse only ablated a small amount of the remaining B layer.

Due to spectral overlap between B and W emission lines at 703.2 nm, 412.2 nm, and 249.7 nm, accurate determination and extraction of net B signals under varying laser pulse conditions are critical. In previous work [27], the method of extracting the net B signal using the equation $S_{B\text{-}net\ signal} = S_{overlap\ region} - k \times S_{substrate}$ was proposed and successfully used to obtain the depth distribution profile of the B signal. k is calculated by the ratio of $S_{overlap\ region}$ to $S_{substrate}$ in the pure W spectrum. Moreover, based on the significant differences in the spatial distribution behaviors of B II and W I, it appears promising to quickly determine the presence of B elements on the W-substrates only using a single laser pulse.

Figs. 10(a) and (b) respectively present the spatial distribution spectra of sample No.1 with a B layer thickness of only 5.6 nm under the 1st and 2nd laser pulses. The spectral results in Fig. 9(a) indicate that the 2nd pulse generates W-substrate signals with no detectable B signal. Therefore, for W, its spatial distribution has a narrow radial distribution, with noticeable W I signals only detected within the −1.4 to 1.4 mm range. In contrast, the broader expansion of the B element allows its signal to remain clearly visible outside the −1.4 to 1.4 mm range. This suggests that in the spatial distribution spectra shown in Fig. 10(a), the region around 703.2 nm within the −1.4 to 1.4 mm range corresponds to the overlap of the B II and W I lines, while outside this range, only the net B II lines is observed. In addition, the spatial distribution spectra of sample No.10 with a B layer thickness of 151.5 nm under the 2nd and 5th laser pulses are also shown in Figs. 10(c) and (d), respectively. The spectra presented under the 2nd laser pulse corresponds to the pure B layer (with no ablation of the W-substrate), while the spectra under the 5th laser pulse corresponds to the W-substrate. It can be observed that when ablating the pure B layer, the B signal is strong enough for the characteristic peaks of B II lines to be detected in the spectra corresponding to each fiber. Therefore, using a spatially resolved method to detect the B layers on the W-substrates enables the rapid and accurate determination of the presence of B signals and the extraction of the net B signal.

3.4. The quantitative calibration curve and LOD for B

In this work, the thickness and amount of the B layer were

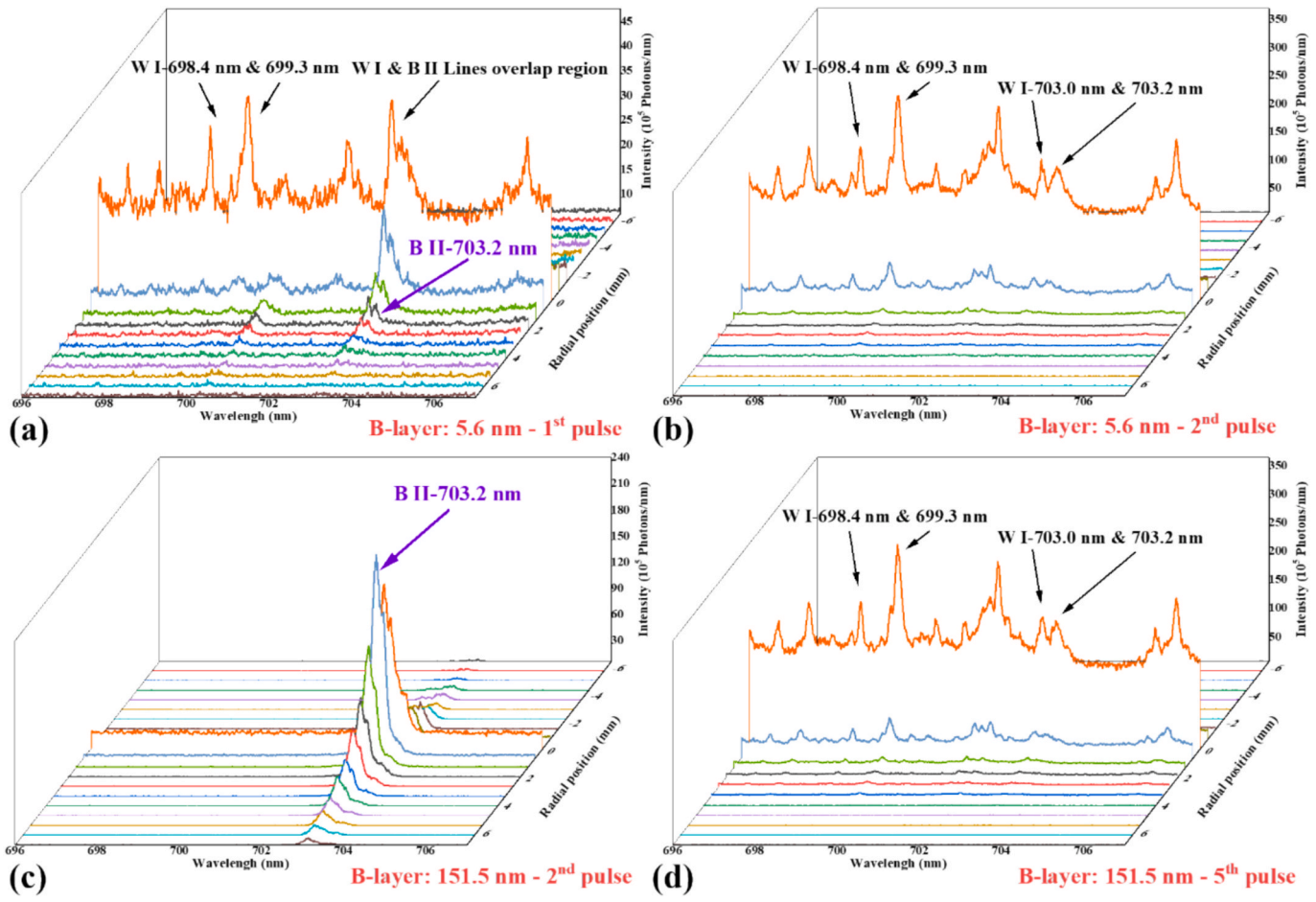

Fig. 10. Spatial characteristics of spectra of B layers (sample-No.1) on the W-substrates under the (a) 1st and (b) 2nd laser pulse. Spatial characteristics of spectra of B layers (sample-No.10) on the W-substrates under the (c) 2nd and (d) 5th laser pulse.

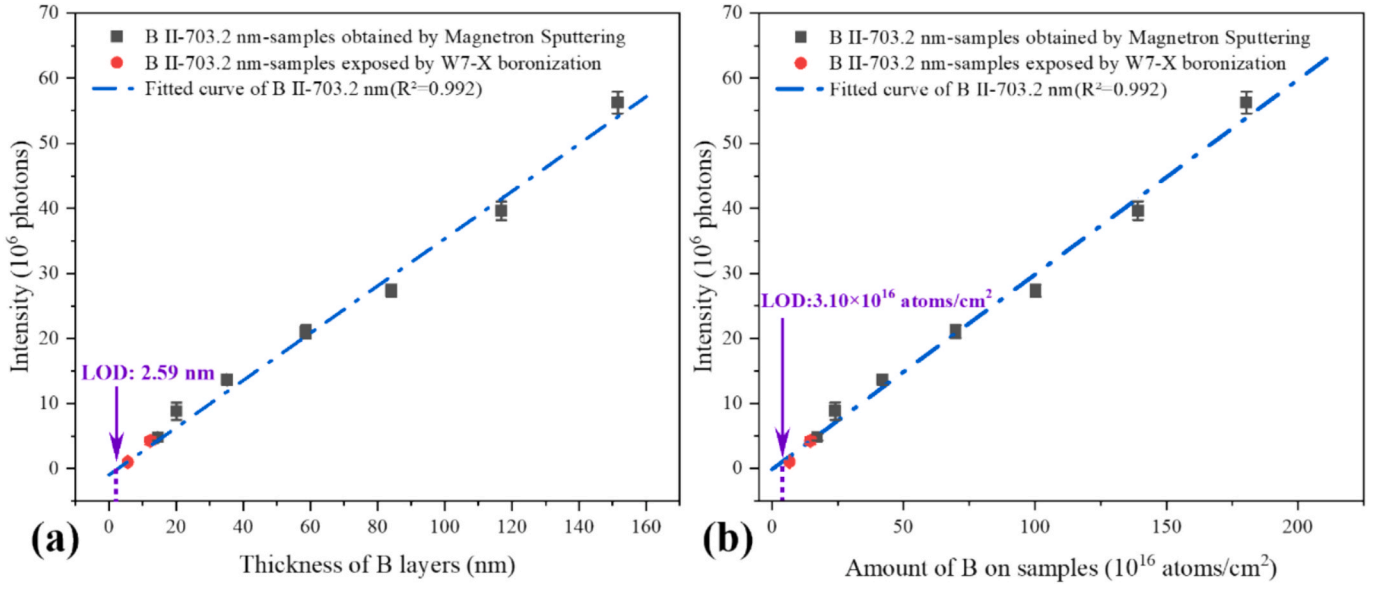

Fig. 11. External standard calibration curve and LOD of B II-703.2 nm versus (a) layer thicknesses and (b) amount of B.

determined based on the FIB-SEM measurement results. At the same time, a depth scan of the B element on the section obtained by FIB cutting was conducted using EDS, which verified the FIB-SEM measurements of the B layer thickness on the W-substrate. The EDS measurements also revealed that O consistently exists in the films, and its depth profile trend is consistent with that of the main element B (92.6 at%). This suggests that the analyzed layer is likely to contain boron oxide. It is assumed that the atomic number density of pure boron layer

is approximately 1.30×10^{23} atoms/cm^3. Since a small portion of the B layer was oxidized, the average atomic number density of B in the deposited layer was calculated to be approximately 1.10×10^{23} atoms/cm^3, based on the atomic percentages of B, O, and W obtained from the EDS analysis (B: 92.6 at%, O: 6.9 at%, W: 0.5 at%).

In previous work [27], the intensity ratio method was initially used for the measurement of two B layers with two different thicknesses (128.4 nm and 276.9 nm). In this work, the external standard calibration curve for B II-703.2 nm under the current experimental conditions was obtained through the extraction of the B signal from the spectra of samples with 9 different B layer thicknesses, as shown in Fig. 11. The net B signal is the sum of the first five laser pulses of the LIBS measurement. Both the B layer samples with different thicknesses obtained through magnetron sputtering and the B layer samples obtained after boronization in W7-X device are in good agreement with the fitted linear calibration curve. The R-squared value of the fitted curve reached 0.992. Therefore, under the present experimental conditions, the thickness and areal number density of the boron layer on W substrates can be determined using Eqs. (2) and (3), respectively:

$$T_{boron} = \left(\left(P_{BII-703.2nm}/10^6\right) + 0.9390\right)/0.3632 \quad (2)$$

$$N_{boron} = \left(\left(P_{BII-703.2nm}/10^6\right) + 0.1132\right)/0.2994*10^6 \quad (3)$$

where T_{boron} (unit: nm) denotes the thickness of the boron layer, $P_{B\ II\text{-}703.2\ nm}$ represents the photons counts of the B II 703.2 nm emission line collected by the LIBS system, and N_{boron} (unit: atoms/cm^2) is the areal number density of the boron layer.

These results demonstrate the feasibility and potential of the LIBS-based approach for quantitative analysis of boron layer thickness. Prior to actual boronization in fusion devices, LIBS measurements will be performed on several standard W-substrate samples with known boron layer thicknesses to establish a reliable calibration curve. Subsequently, using the identical LIBS measurement parameters, the samples after boronization could be measured to determine the thickness or the amount of boron at specific location. Nonetheless, considering both the EDS results and relevant reports, the B layers examined in this study are most likely to contain boron oxides [35,36]. This finding indicates that the present calibration curve is specifically applicable to oxidized B layers deposited on W-substrates. Future work will combine X-ray Photoelectron Spectroscopy (XPS) with ps-LIBS to systematically investigate and characterize a broader range of B chemical states (e.g., B-oxide, B-D/T, B-O-D/T, B-C, B-O-C, B-W) formed under fusion-relevant conditions, thereby enabling a more comprehensive validation and extension of the applicability of LIBS for in-situ analysis of B-containing layers.

The calibration curve allows for the determination of the LOD for B (B II-703.2 nm) on the W-substrates under the current LIBS experimental conditions. The calculation of the LOD is given by Eq. (4) [37,38]:

$$LOD = \frac{3\sigma}{s} \quad (4)$$

Where σ is the standard deviation of the spectral background. The value of σ was calculated in the background ranges from 704.18 nm to 705.18 nm for the selected LIBS spectra. s is the slope of the external standard calibration curve of B. Based on Eq. (4), the LOD for the thickness and the amount of B layer on the W-substrate using ps-LIBS were calculated to be 2.59 nm and 3.10×10^{16} atoms/cm^2 (the diameter of laser spot is about 488 μm), respectively.

4. Conclusion

In this work, the relationship between the photons of B II-703.2 nm emission, laser energy, and laser spot size was systematically characterized, and the optimal laser fluence (9.6 J/cm^2) was determined for a ps-laser at 355 nm. The spatiotemporal dynamics of B II-703.2 nm and W I-699.4 nm were then investigated using a linear array fiber bundle, and the results were consistent with those obtained from fast imaging techniques. By utilizing the significant difference in the spatial distribution behaviors of B II and W I species, the presence of B could be quickly identified with a single laser pulse. By extracting the net B signal from the spectra for different laser pulses and using the thicknesses information of B layers measured by FIB-SEM, a quantitative calibration curve for the B II-703.2 nm line of B layers on W-substrate was obtained. The limit of detection (LOD) for the thickness and the amount of the B layers on the W-substrates were calculated to be 2.59 nm and 3.10×10^{16} atoms/cm^2, respectively. The results that the samples obtained by magnetron sputtering and those from W7-X after boronization both aligned with the quantitative calibration curve provides a promising solution for *in situ*, rapid determination of the B layer thickness and content at different locations after boronization in fusion devices.

CRediT authorship contribution statement

Huace Wu: Writing – original draft, Methodology, Investigation, Conceptualization. **Rongxing Yi:** Visualization, Data curation. **Sebastijan Brezinsek:** Writing – review & editing, Project administration, Data curation. **Anne Houben:** Resources. **Marcin Rasinski:** Visualization. **Rui Ding:** Methodology. **Matej Mayer:** Resources. **Gennady Sergienko:** Software. **Timo Dittmar:** Validation. **Hongbin Ding:** Writing – review & editing, Supervision, Funding acquisition.

Declaration of competing interest

The authors declare that they have no known competing financial interests or personal relationships that could have appeared to influence the work reported in this paper.

Acknowledgements

This research was supported by the National Key R&D Program of China (No. 2023YFF0714901), the National Natural Science Foundation of China (Nos.12375208). The authors gratefully acknowledge the support of the Institute of Energy, Hefei Comprehensive National Science Center (Anhui Energy Laboratory) (No.25KZS217). This work has been carried out within the framework of the EUROfusion Consortium, funded by the European Union via the Euratom Research and Training Programme (Grant Agreement No 101052200 - EUROfusion). Views and opinions expressed are however those of the author(s) only and do not necessarily reflect those of the European Union or the European Commission. Neither the European Union nor the European Commission can be held responsible for them.

Data availability

Data will be made available on request.

References

[1] J. Winter, H.G. Esser, L. Konen, et al., BORONIZATION IN TEXTOR, J. Nucl. Mater. 162 (1989) 713–723.
[2] G.L. Jackson, J. Winter, T.S. Taylor, et al., REGIME OF VERY HIGH CONFINEMENT IN THE BORONIZED DIII-D TOKAMAK, Phys. Rev. Lett. 67 (1991) 3098–3101.
[3] J.S. Hu, X.M. Wang, J.H. Li, et al., Vacuum and wall conditioning system on EAST, Fusion Eng. Des. 84 (2009) 2167–2173.
[4] N. Ashikawa, K. Kizu, J. Yagyu, et al., Comparison of boronized wall in LHD and JT-60U, J. Nucl. Mater. 363 (2007) 1352–1357.
[5] T. Klinger, T. Andreeva, S. Bozhenkov, et al., Overview of first Wendelstein 7-X high-performance operation, Nucl. Fusion 59 (2019) 11, 112004.
[6] J. Winter, Wall conditioning in fusion devices and its influence on plasma performance, Plasma Phys. Controlled Fusion 38 (1996) 1503–1542.
[7] A. Kallenbach, R. Dux, M. Mayer, et al., Non-boronized compared with boronized operation of ASDEX Upgrade with full-tungsten plasma facing components, Nucl. Fusion 49 (2009) 045007.

[8] A. Gallo, P. Moreau, D. Douai, et al., Wall conditions in WEST during operations with a new ITER grade, actively cooled divertor, Nucl. Mater. Energy 41 (2024) 101741.
[9] R.A. Pitts, A. Loarte, T. Wauters, et al., Plasma-wall interaction impact of the ITER re-baseline☆, Nucl. Mater. Energy 42 (2025) 28, 101854.
[10] K. Schmid, T. Wauters, Full W ITER: Assessment of expected W erosion and implications of boronization on fuel retention, Nucl. Mater. Energy 41 (2024) 11, 101789.
[11] W. Xu, Z. Wang, Z. Sun, et al., Investigation of boron powder flow rates on real-time wall, Nucl. Mater. Energy 42 (2025) 6, 101869.
[12] T. Nakano, S. Higashijima, H. Kubo, et al., Boronization effects using deuterated-decaborane (B10D14) in JT-60U, J. Nucl. Mater. 313 (2003) 149–152. Pii s0022-3115(02)01402-2.
[13] S. Abe, M.J. Simmonds, A. Bortolon, et al., Deuterium retention behaviors of boronization films at DIII-D divertor surface, Nucl. Mater. Energy 42 (2025) 6, 101855.
[14] G. Bodner, A. Gallo, A. Diallo, et al., Initial results from boron powder injection experiments in WEST lower single null L-mode plasmas, Nucl. Fusion 62 (2022) 14, 086020.
[15] J.A. Snipes, L.R. Baylor, A. Bortolon, et al., Initial design concepts for solid boron injection in ITER, Nucl. Mater. Energy 41 (2024) 6, 101809.
[16] S. Masuzaki, M. Shoji, F. Nespoli, et al., Glow Discharge Boronization and Real-Time Boronization Using an Impurity Powder Dropper in LHD, Nucl. Mater. Energy 42 (2025) 101843.
[17] G.S. Maurya, A. Marín-Roldán, P. Veis, et al., A review of the LIBS analysis for the plasma-facing components diagnostics, J. Nucl. Mater. 541 (2020) 19, 152417.
[18] C. Li, L.Y. Sun, Z.H. Hu, et al., An in situ diagnostic method for monitoring of fuel retention on the first wall under long-pulse operation of experimental advanced superconducting tokamak, Phys. Scr. T171 (2020) 7, 014069.
[19] Z.H. Hu, X. Bai, H.C. Wu, et al., Quantitative analysis of impurities deposited on the Plasma-Facing Components of EAST tokamak using a portable LIBS device, Nucl. Mater. Energy 41 (2024) 7, 101785.
[20] A.G. Razdobarin, O.S. Medvedev, I.M. Bukreev, et al., Laser Diagnostics of Content of Hydrogen Isotopes in the Globus-M2 Tokamak Wall, Plasma Phys. Rep. 50 (2024) 667–677.
[21] M. Ladygina, W. Gromelski, P. Gasior, et al., LIBS diagnostics of Be-based samples with different gas impurities, Phys. Plasmas 31 (2024) 6, 063501.
[22] A.M. Roldan, V. Dwivedi, M. Pisarc, et al., LIBS investigation of metals suitable for plasma-facing components: Characteristics and comparison of picosecond and nanosecond regimes, Fusion Eng. Des. 172 (2021) 8, 112898.
[23] A.M. Roldán, V. Dwivedi, M. Veis, et al., Quantification of hydrogen isotopes by CF-LIBS in a W-based material (WZr) at atmospheric pressure: from ns towards ps, Phys. Scr. 96 (2021) 9, 124061.
[24] M.L. Sankhe, A. Favre, J.B. Sirven, et al., Development of fibered LIBS device for tokamak Plasma Facing Components characterization, Fusion Eng. Des. 197 (2023) 5, 114077.
[25] S. Mittelmann, J. Oelmann, S. Brezinsek, et al., Laser-induced ablation of tantalum in a wide range of pulse durations, Appl. Phys. A-Mater. Sci. Process. 126 (2020) 7, 672.
[26] D. Zhao, S. Brezinsek, R. Yi, et al., Investigation of boron distribution and material migration on the W7-X divertor by picosecond LIBS, Phys. Scr. 97 (2022) 10, 024005.
[27] H.C. Wu, R.X. Yi, A. Houben, et al., Study of spectral features and depth distributions of boron layers on tungsten substrates by ps-LIBS in a vacuum environment, Nucl. Mater. Energy 41 (2024) 12, 101812.
[28] A. Goriaev, T. Wauters, R. Brakel, et al., Wall conditioning at the Wendelstein 7-X stellarator operating with a graphite divertor, Phys. Scr. T171 (2020) 7, 014063.
[29] S. Sereda, S. Brezinsek, E. Wang, et al., Impact of boronizations on impurity sources and performance in Wendelstein 7-X, Nucl. Fusion 60 (2020) 8, 086007.
[30] M. Mayer, M. Balden, T. Bräuer, et al., Properties of boron layers deposited during boronisations in W7-X, Nucl. Mater. Energy 41 (2024) 8, 101778.
[31] H.C. Wu, C. Li, D. Wu, et al., Spatiotemporal dynamic characterization of the laser-induced plasma of a mixed material (WCCu) under variable ablation angles in a vacuum, J. Anal. At. Spectrom 37 (2022) 2069–2081.
[32] P. Liu, J.M. Liu, D. Wu, et al., Study of Spark Discharge Assisted to Enhancement of Laser-Induced Breakdown Spectroscopic Detection for Metal Materials, Plasma Chem. Plasma Process. 38 (2018) 803–816.
[33] M.T. Taschuk, Y. Godwal, Y.Y. Tsui, et al., Absolute characterization of laser-induced breakdown spectroscopy detection systems, Spectroc. Acta Pt. B-Atom. Spectr. 63 (2008) 525–535.
[34] H.C. Wu, D. Wu, C. Li, et al., Effect of laser ablation angles on the ablated depth/mass and spectral intensity of laser-induced plasma on EAST-like plasma-facing materials in a vacuum, Spectroc. Acta Pt. B-Atom. Spectr. 202 (2023) 11, 106647.
[35] R.M. Saha, K. Banerjee, A. Banerjee, et al., Investigation of spitting effect in the boron target preparation using vapour deposition technique, Vacuum 230 (2024) 9, 113642.
[36] B. Wicher, J. Palisaitis, V. Rogoz, et al., Synthesis of Hard Boron Thin Films by Low Frequency Magnetron Sputtering, Mater. Des. 257 (2025) 15, 114404.
[37] M.A. Ismail, H. Imam, A. Elhassan, et al., LIBS limit of detection and plasma parameters of some elements in two different metallic matrices, J. Anal. At. Spectrom 19 (2004) 489–494.
[38] A.M. Popov, F. Colao, R. Fantoni, Spatial confinement of laser-induced plasma to enhance LIBS sensitivity for trace elements determination in soils, J. Anal. At. Spectrom 25 (2010) 837–848.